SCIENCE CHINA
Technological Sciences

November 2012 Vol.55 No.11: 3213–3222
doi: 10.1007/s11431-012-5006-3

Direct numerical simulation of turbulent flow over backward-facing at high Reynolds numbers

DING DaoYang & WU ShiQiang*

State Key Laboratory of Hydrology-Water Resources and Hydraulic Engineering, Nanjing Hydraulic Research Institute, Nanjing 210029, China

Received January 28, 2012; accepted April 25, 2012; published online August 30, 2012

Direct numerical simulation (DNS) was performed for the first time to study the flow over a backward-facing step at a high Reynolds number on a coarse grid. The flow over backward-facing step is the typical turbulent flow controlled by large eddy, in which the effect of small eddy could be negligible as an approximation. The grid dimension could easily satisfy the resolution requirement to describe the characteristics of a large eddy flow. Therefore, direct numerical simulation of N-S equations to obtain the turbulent flow field on the coarse grid could be realized. Numerical simulation of a two-dimensional flow over a backward-facing step at a Reynolds number Re=44000 was conducted using Euler-Lagrange finite element scheme based on the efficient operator-splitting method (OSFEM). The flow field was descretized by triangle meshes with 16669 nodes. The overall computational time only took 150 min on a PC. Both the characteristics of time-averaged and instantaneous turbulent flow were simultaneously obtained. The analysis showed that the calculated results were in good agreement with the test data. Hence, the DNS approach could become the reality to solve the complex turbulent flow with high Reynolds numbers in practical engineering.

DNS, the flow over backward-facing step, high Reynolds number

Citation: Ding D Y, Wu S Q. Direct Numerical Simulation of turbulent flow over backward-facing step at high Renolds numbers. Sci China Tech Sci, 2012, 55: 3213–3222, doi: 10.1007/s11431-012-5006-3

1 Problems introduction

Turbulent flow is one of the common phenomena in fluid movement in engineering practice, its numerical simulation has been one of the most difficult problems in fluid mechanics for a long time. At present, there exist three solution techniques. The first one is using time-averaged N-S equations with the aid of a semi-empirical approach modeling the turbulent effect, and is called RANS method, of which k-ε model is a widely used method in engineering. However, this method could only produce time-averaged flow field. The second solution technique is based on partial space-averaged N-S equation, called LES method, which can produce instantaneous flow field, but still needs a semi-empirical approach for modeling the turbulent effect. The third one is a direct simulation of turbulent flow by solving N-S equations, called DNS method, which can directly simulate complicated instantaneous turbulent flow phenomena without using any other model to simulate turbulent effect, and is generally recognized as the most ideal approach.

The study of DNS method was started in early 1970s. Orszag SA and Patterson GS initiated the computation of 3D isotropic turbulent flow. With the development of numerical simulation and computer technology, some progress has been made in DNS studies, from simple isotropic turbulent flow in early days to anisotropic boundary flow, and from incompressible flow to compressible flow [1–6]. Only

*Corresponding author (email: sqwu@nhri.cn)

© Science China Press and Springer-Verlag Berlin Heidelberg 2012

a few research results have been found in the study of complex turbulent flow with boundary separation commonly encountered in practical engineering, and all with Reynolds number below 5000. In 1998, based on time-splitting method, Hung et al. [7] simulated 3D incompressible turbulent flow over backward-facing step using finite difference method and stagger-grid mesh of about 10^8 nodes. In 2008, Sengupta et al. [8] reported the results of simulation of 3D compressible turbulent flow over backward-facing step using spectrum method.

Although DNS method is the best in simulating turbulent flow, why cannot it be used to solve practical engineering problems? The reason is that first of all, discrete mesh dimension must satisfy the Kolmogorov micro dimension requirement. It is held that there exist eddies of all dimensions in the turbulent flow, hence, in order to satisfy the resolution requirement of small eddies, mesh dimension should satisfy the micro dimension requirement. For the 3D problems the number of mesh nodes must be up to 10^9–10^{11}, with the increase of Reynolds number, the mesh dimension is required to be smaller and time step becomes smaller accordingly; thus the computation effort is enormous, which can not be realized even by modern super computers. Currently, DNS method is generally used as a research tool to study turbulence mechanism, to conduct numerical tests on artificially schematized turbulent flow, and to obtain the results of turbulence mechanism, not obtainable from physical tests, so as to finally provide a basis for turbulent flow model studies [9].

If DNS is directly used to simulate turbulent flow at a high Reynolds number on coarser grids without considering the micro dimension requirement of Kolmogorov, what would happen? Is the numerical solution totally distorted? Or the computer would overflow and can not continue in the process of numerical calculation? There is no such relevant report up to now, which urges the authors' to make attempts on this issue.

In the natural turbulent flow, eddies of all dimensions, large or small, do not play the same role, hence it is not necessary to simulate the turbulent flow fields for all eddy dimensions. For a gradually varying boundary-flow, when the flow has no boundary separation, there obviously exist small eddies only, which play the main role in the flow field; for a suddenly varying complex turbulent flow leading to the boundary separation due to suddenly boundary change, the resultant eddies of large dimensions play the dominant role in the flow field, while eddies of small dimensions play the secondary role. The turbulent flow over a backward-facing step often occuring in practical engineering is a typical flow controlled by large eddies, which can be described by using coarse grids to satisfy the resolution requirement for large eddies. This approach can be used as an approximate engineering method regardless of Kolmogorov's micro dimension requirement.

Another important factor constraining the development of DNS is the difficulty in the numerical solution of N-S equations at a high Reynolds number, for which many solution methods for N-S equations at a low Reynolds number become unusable. As the convection term in the equation is a nonlinear term, which is the source generating turbulent flow, with the increase of Reynolds number, the effect of nonlinearity increases, which needs a high-accuracy discrete method to adapt to the high nonlinearity. At present, the DNS numerical method for turbulent flow is mainly a finite difference method, which focuses on high accuracy in time and space. Practice shows that the accuracy of finite difference scheme affects grid dimension largely. The grid dimension of a fourth-order accuracy scheme is four times greater than a second-order accuracy scheme [10]. The idealness of a compact finite difference scheme higher than fourth-order accuracy can compare to that of the spectrum method [11]. The spectrum method with approximate solution function of very high smoothness, and with application of fast Fourier transformation, is a high efficient method for DNS method to simulate turbulent flow, but is not applicable to complex geometrical boundary. The finite element method, though applicable to complex boundary, is seldom used to solve N-S equations of flow with a high Reynolds number. Although the upwind finite element scheme is used for solution of convection operator, it is only applicable to flow at a lower Reynolds number. Whatever method is used at present, the treatment of nonlinear convection term remains difficult and vital in computation. In 2006, a smooth particle hydrodynamic method (SPH method) was reported to compute the 2D incompressible turbulent flow over backward-facing step by adopting pure Lagrangian method to directly solve N-S equations under Lagrangian coordinate, which avoided the difficulty in solving the nonlinear convection term [12].

The authors, in using k-ε model to simulate turbulent flow over backward-facing step, developed a kind of SEL method [13], which is a finite element method combining the Euler-Lagrange approach based on the operator-splitting method (time-splitting method). The method takes the advantages of Lagrange method to avoid the difficulty in the treatment of nonlinear term, and maintains the conventional simplicity of Euler method. It is hoped that this method can fit DNS method to simulate turbulent flow at a high Reynolds number. The method has therefore been used to directly solve N-S equations on normal grid mesh so as to simulate complex turbulent flow at a high Reynolds number controlled by large eddies. This method is called SEL-DNS method in this paper.

2 Basic equations and problems to be sloved

As reported in ref. [14], on the Conference on Complex Turbulent Flow in 1980 in Stanford, USA, it was suggested that the test conditions of turbulent flow over backward-

facing step in ref. [15] should be taken as the verification object of the numerical modeling study of complex turbulent flow. The test was conducted in a rectangular wind tunnel with a width of W=96 cm and a step height H=3.81 cm, extending from bell-shape transitional part to the flat and straight channel. The Reynolds number is about 44000 based on inflow velocity U_0 =18.2 m/s and step height H. The channel height upstream of the step H_1=2H and that downstream of the step H_2 =3H, and the expansion ratio H_2/H_1=1.5, and channel width W=16H, based on which the flow can be basically regarded as a 2D flow. In this paper, the above conditions are taken as the study object. As shown in Figure 1, the inflow boundary is placed at 4H upstream the step and the outflow cross section at 2H downstream the step.

It is assumed that characteristic length is step height H and characteristic velocity is free flow velocity at entrance cross section U_0. The following dimensionless quantities are introduced:

$$\begin{aligned} &\tilde{U}=\frac{U}{U_0},\tilde{V}=\frac{V}{U_0},\tilde{P}=\frac{P}{U_0^2/2g},\tilde{t}=t\frac{U_0}{H},\\ &Re=\frac{U_0H}{\nu},\tilde{x}=\frac{x}{H},\tilde{y}=\frac{y}{H}, \end{aligned} \tag{1}$$

where pressure P is represented by pressure head. For the sake of convenience, in the following, the curved dash on the dimensionless quantity is omitted. The dimensionless 2D incompressible N-S equations are derived as

$$\frac{\partial U}{\partial x}+\frac{\partial V}{\partial y}=0, \tag{2}$$

$$\begin{aligned} &\frac{\partial U}{\partial t}+U\frac{\partial U}{\partial x}+V\frac{\partial U}{\partial y}=-\frac{1}{2}\frac{\partial P}{\partial x}+\frac{1}{Re}\left(\frac{\partial^2U}{\partial x^2}+\frac{\partial^2U}{\partial y^2}\right),\\ &\frac{\partial V}{\partial t}+U\frac{\partial V}{\partial x}+V\frac{\partial V}{\partial y}=-\frac{1}{2}\frac{\partial P}{\partial y}+\frac{1}{Re}\left(\frac{\partial^2V}{\partial x^2}+\frac{\partial^2V}{\partial y^2}\right). \end{aligned} \tag{3}$$

Unless specially pointed out, the parameters without curved dash in the paper are regarded as dimensionless parameters.

Giving solution conditions for quasi-linear partial differential equation is a difficult problem. By now, the well-posedness of solution of mixed operator equation of nonlinear term is not mathematically verified, but only verified empirically through numerical tests. To well-pose the boundary and initial conditions of N-S equations is almost impossible, especially the determination of inflow boundary conditions. In simulating turbulent flow, DNS method is required to give the stochastic pulsation process of flow velocity at the entrance to trigger pulsation in the flow field, which can hardly be satisfied. Various methods are tried to give an approximate value. In fact, the instability of flow at a high Reynolds number is the inherent characteristic of N-S equations, by which the computational results of flow field pulsation can be obtained even without the inflow stochastic velocity pulsation. In this paper, the inflow boundary adopts steady velocity distribution without stochastic pulsation momentum:

$$U_i=U_0(1-\exp(-my)), \tag{4}$$

where m is a constant and is chosen as 35 here.

As the upper and lower ends of the inflow boundary are both non-slip boundaries, the velocity distribution at the central line of the inflow boundary is symmetrical. Figure 2 is the distribution obtained from eq. (4). The inflow boundary pressure satisfies natural boundary conditions, the upper and lower boundaries are solid wall boundaries, velocity is treated as non-slip boundary, and pressure is still taken as natural boundary. At the exit, velocity is treated according to non-reflection boundary conditions, pressure is a boundary condition, and P=0. The initial condition is stationary flow field and all the flow parameters are zero.

3 Numerical solution technique of SEL-DNS

In the SEL method developed by the authors in ref. [14], the momentum transport equation containing complex operators is split according to the characteristics of operators to adapt to suitable numerical methods: Lagrange method is used to solve nonlinear convection operator and Euler method is applied to solve linear diffusion operator, the way of which can be called a mixed Euler-Lagrange approach. This approach was successfully applied to the numerical solution of 2D and 3D flows in wide and shallow rivers [16, 17].

To adapt to DNS method, an adjusting factor is introduced in splitting of operators, and the momentum equation

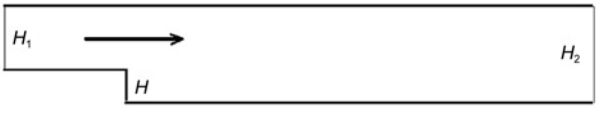

Figure 1 Schematic diagram of computation domain and boundary.

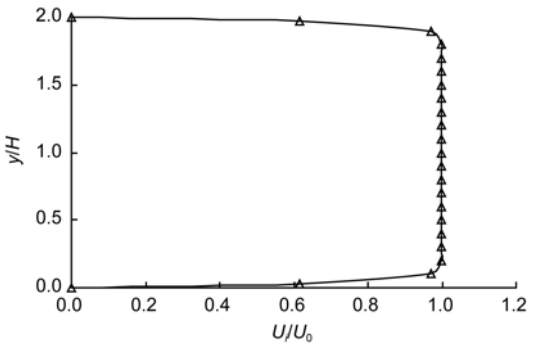

Figure 2 Velocity distribution at entrance cross section.

is then solved by three steps: convection step (eq. (5)), propagation step (eq. (6)) and diffusion step (eq. (7)):

$$\begin{aligned}\frac{\partial U}{\partial t}+U\frac{\partial U}{\partial x}+V\frac{\partial U}{\partial y}&=-\frac{\alpha}{2}\frac{\partial p}{\partial x},\\ \frac{\partial V}{\partial t}+U\frac{\partial V}{\partial x}+V\frac{\partial V}{\partial y}&=-\frac{\alpha}{2}\frac{\partial p}{\partial y},\end{aligned}\tag{5}$$

$$\begin{aligned}\frac{\partial U}{\partial t}&=-\frac{1}{2}(1-\alpha)\frac{\partial p}{\partial x},\\ \frac{\partial V}{\partial t}&=-\frac{1}{2}(1-\alpha)\frac{\partial p}{\partial y},\end{aligned}\tag{6}$$

$$\begin{aligned}\frac{\partial U}{\partial t}&=\frac{1}{Re}\left(\frac{\partial^2 U}{\partial x^2}+\frac{\partial^2 U}{\partial y^2}\right),\\ \frac{\partial V}{\partial t}&=\frac{1}{Re}\left(\frac{\partial^2 V}{\partial x^2}+\frac{\partial^2 V}{\partial y^2}\right),\end{aligned}\tag{7}$$

where α is a adjusting factor. When α=0, which is the splitting scheme in SEL method in ref. [13], α=0.025 is chosen in this paper.

It is found in the numerical test by the authors that when DNS is used to solve the turbulent flow at a high Reynolds number, the solution is very sensitive to some detail of the computation method, leading to unstable or unrealistic solutions. When the adjusting factor is introduced, the solution of DNS may be well controlled.

In one time step, time advancement can be completed by above three steps. The pressure at lower time step, a known value, is used for the pressure term at the right side of the convection step (eq. (5)). When Lagrange approach is used for solution, eq. (5) can be written as follows:

$$\begin{aligned}\frac{\mathrm{d}U}{\mathrm{d}t}&=-\frac{\alpha}{2}\frac{\partial p^{(n)\Delta t}}{\partial x},\\ \frac{\mathrm{d}V}{\mathrm{d}t}&=-\frac{\alpha}{2}\frac{\partial p^{(n)\Delta t}}{\partial y}.\end{aligned}\tag{8}$$

Taking point *i* in Figure 3 as an example, in the elements surrounding the point, one should try to find its convection element M and corresponding convection point D. The particle path line equations of point D are

$$\begin{aligned}\frac{\mathrm{d}x}{\mathrm{d}t}&=U,\\ \frac{\mathrm{d}y}{\mathrm{d}t}&=V.\end{aligned}\tag{9}$$

The value at any point (x, y) in the M^{th} element surrounding i is represented by linear interpolation:

$$x=\sum_{i=1}^{3}L_i x_i,\ y=\sum_{i=1}^{3}L_i y_i.\tag{10}$$

If U and V in the element also use linear interpolation, it is easy to get area coordinates L_1, L_2 and L_3 at point D. If the three area coordinates are greater than 0 and less than 1, this shows point D is within the element under investigation, which can be taken as convection element M, and its corresponding point D is the convection point. Velocity at point D can be calculated by

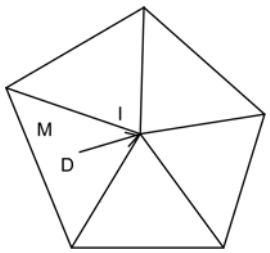

Figure 3 Flow particle convection at convection element D.

$$\begin{aligned}U_d&=\sum_{i=1}^{3}L_i U_i^{n\Delta t},\\ V_d&=\sum_{i=1}^{3}L_i V_i^{n\Delta t}.\end{aligned}\tag{11}$$

The flow particle at point D at time n arrives at point I after Δt. From eq. (8), one can obtain the value of point i after convection at time t_{n+1}

$$\begin{aligned}U_i^c&=U_d^{n\Delta t}-\frac{\alpha\Delta t}{2}\frac{\partial p^{(n)\Delta t}}{\partial x},\\ V_i^c&=V_d^{n\Delta t}-\frac{\alpha\Delta t}{2}\frac{\partial p^{(n)\Delta t}}{\partial y}.\end{aligned}\tag{12}$$

It can be seen that as the Lagrange approach is used in the convection step, the difficulty in treating nonlinearity is thus avoided, and the computational stability and accuracy are effectively increased. Therefore, the approach is suitable for the solution of N-S equations at high Reynolds numbers.

For the solution of the pressure propagation step, an explicit finite element method is used. The following equations are derived from eq. (6):

$$\begin{aligned}U_i^p&=U_i^c-\frac{(1-\alpha)}{2}\Delta t\frac{\partial P^{(n+1)\Delta t}}{\partial x},\\ V_i^p&=V_i^c-\frac{(1-\alpha)}{2}\Delta t\frac{\partial P^{(n+1)\Delta t}}{\partial y},\end{aligned}\tag{13}$$

where (U^p, U^c, V^p, V^c) represent the corresponding physical values after convection and pressure propagation, respectively. To obtain the pressure at higher time step, x, y are derived respectively from the above equations so as to satisfy the continuity equation after pressure propagation. Thus we get

$$\frac{\partial^2 P^{(n+1)\Delta t}}{\partial x^2}+\frac{\partial^2 P^{(n+1)\Delta t}}{\partial y^2}=\frac{2}{(1-\alpha)\Delta t}\left(\frac{\partial U_c}{\partial x}+\frac{\partial V_c}{\partial y}\right).\tag{14}$$

The right side of the above is known as a typical pressure

Poisson equation, which can be easily solved by the implicit finite element method. The Galerkin weighted-residual method and pressure Poisson equation (eq. (14)) are equivalent to solving the following integral equation:

$$\begin{aligned}&\iint_A (\frac{\partial N}{\partial x}\frac{\partial P^{(n+1)\Delta t}}{\partial x}+\frac{\partial N}{\partial y}\frac{\partial P^{(n+1)\Delta t}}{\partial y})\mathrm{d}\Omega = \\ &\int_S N\frac{\partial P^{(n+1)\Delta t}}{\partial n}\mathrm{d}s-\frac{2}{(1-\alpha)\Delta t}\iint_A N(\frac{\partial U_c}{\partial x}+\frac{\partial V_c}{\partial y})\mathrm{d}\Omega.\end{aligned} \tag{15}$$

Using shape function L as weighted function N, the linear positive definite symmetric sparse coefficient matrices can be derived, and it can be solved by use of L-R method easily. After the pressure at higher time step is solved, velocity at higher time step $(U_i^{(n+1)}, V_i^{(n+1)})$ can be easily obtained from eq. (13) after the effect of propagation of the pressure .

Diffusion step can be solved by using implicit finite element method. From eq. (7), one can obtain

$$\begin{aligned}U^{(n+1)} &= U_p+\frac{\Delta t}{Re}(\frac{\partial^2 U^{(n+1)}}{\partial x^2}+\frac{\partial^2 U^{(n+1)}}{\partial y^2}), \\ V^{(n+1)} &= V_p+\frac{\Delta t}{Re}(\frac{\partial^2 V^{(n+1)}}{\partial x^2}+\frac{\partial^2 V^{(n+1)}}{\partial y^2}).\end{aligned} \tag{16}$$

The Galerkin method can be used to solve the following integral equations:

$$\begin{aligned}&\iint_A NU^{(n+1)}\mathrm{d}\Omega+\frac{\Delta t}{Re}\iint_A(\frac{\partial N}{\partial x}\frac{\partial U^{(n+1)}}{\partial x}+\frac{\partial N}{\partial y}\frac{\partial U^{(n+1)}}{\partial y})\mathrm{d}\Omega = \\ &\iint_A NU_p^{(n+1)}\mathrm{d}\Omega+\frac{\Delta t}{Re}\int_S N\frac{\partial U^{(n+1)}}{\partial n}\mathrm{d}s, \\ &\iint_A NV^{(n+1)}\mathrm{d}\Omega+\frac{\Delta t}{Re}\iint_A(\frac{\partial N}{\partial x}\frac{\partial V^{(n+1)}}{\partial x}+\frac{\partial N}{\partial y}\frac{\partial V^{(n+1)}}{\partial y})\mathrm{d}\Omega = \\ &\iint_A NV_p^{(n+1)}\mathrm{d}\Omega+\frac{\Delta t}{Re}\int_S N\frac{\partial V^{(n+1)}}{\partial n}\mathrm{d}s.\end{aligned} \tag{17}$$

4 Numerical test results of SEL-DNS

The computational parameters of 2D flow over a backward-facing step are determined according to the test parameters in ref. [10]. Reynolds number Re based on flow velocity at entrance U_0 and step height H is 44000. The flow field is discretized by triangular element in the computation. To simplify the treatment of computational results, a uniform rectangular mesh is adopted at first, then the rectangular mesh is split into a triangular mesh afterwards. To avoid accumulation of system errors, alternate splitting triangle mesh is used as shown in Figure 4. Two kinds of meshes are compared. In Mesh 1, $\Delta x = 0.167H$, $\Delta y = 0.1H$, number of nodes is 4255, and number of elements is 8160; in Mesh 2, which is a double finer mesh, $\Delta x = 0.0833H$, $\Delta y = 0.05H$, number of nodes is 16669, and number of elements is 32640. The numerical test shows that the computational results of the two meshes are close to each other, but Mesh 2, due to its higher resolution, is smoother. Unless otherwise stated, the computational results described below are from the test of Mesh 2. Time step Δt is $0.025H/U_0$. The test starts from stationary flow field and the total time of the test T_e is $300H/U_0$. The trial test shows that after T_0 =$150H/U_0$, each parameter of the flow field starts to approach a steady trantient process. Therefore, for time averaged statistics, 5000 instantaneous values are adopted in the time period $150H/U_0$ from T_0 to T_e as statistic samples for analysis.

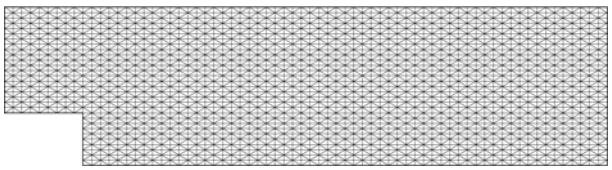

Figure 4 Grid splitting (partial) in computation domain.

4.1 Point pressure behind the step and velocity fluctuation characteristics with time

Although the boundary conditions are given according to steady flow conditions, the parameters of the flow field behind the step pulsate obviously. The pressure and velocity pulsation at the node of x=5.33H and y=1/3H downstream the step in Figure 5 shows that both velocity and pressure pulsate with time, with their main frequencies being comparatively consistent.

4.2 Instantaneous and time-averaged characteristics of velocity in flow field

The computational results show that the velocity at any point in the computational domain in 20H behind the step fluctuates with time, and that quite a few large-scale eddies occur in a relatively large area behind the step, but in 8H behind the step the fluctuation becomes even more intensive and large eddies occur at a higher frequency. With the increase of the distance from the step, large eddies occur at a lower frequency, and few eddies are found adjacent to the upper and lower solid walls of the step and soon disappear. Figure 6 gives nine instantaneous velocity vector fields in the region 8H behind the step, showing that at least few eddies deform, expand, contract, re-occur and disappear with time, thus showing a coherent structure nature. After time-averaging the instantaneous velocity, the time-averaged flow pattern is totally different from instantaneous flow field, showing a good order. Figure 7 gives the time averaged flow field behind the step, showing there is only one large-eddy area. The location of its end point is the reattachment point, and its distance from the step is the reattachment length, which is generally regarded as the recircu-

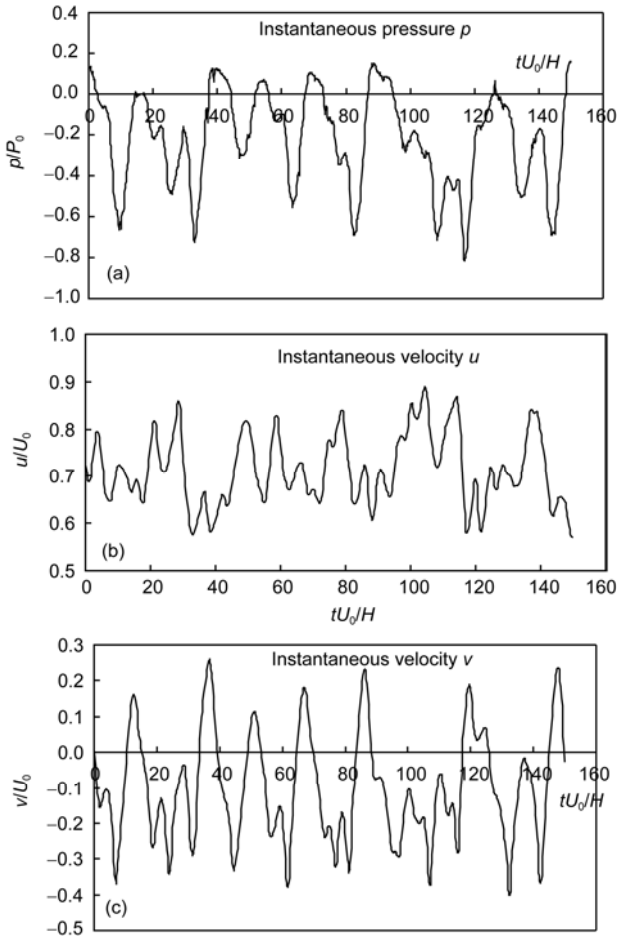

Figure 5 Pulsation process of the pressure at center and velocity in eddy area behind the step.

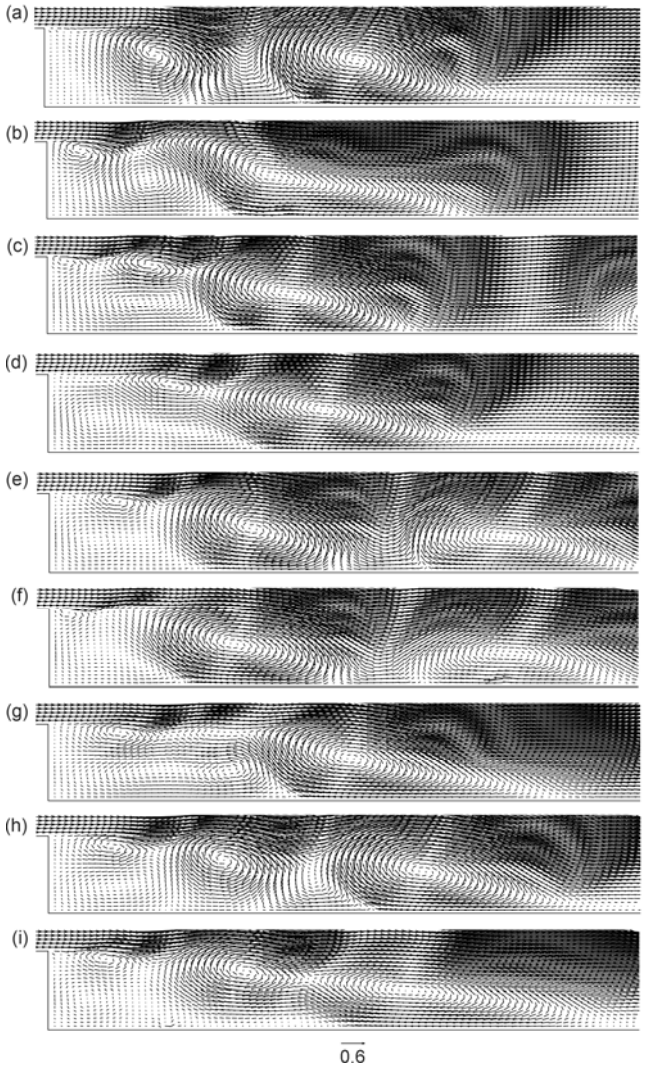

Figure 6 Instantaneous flow field behind the step. (a) T=180H/U_0; (b) T=195H/U_0; (c) T=210H/U_0; (d) T=225H/U_0; (e) T=240H/U_0; (f) T=255H/U_0; (g) T=270H/U_0; (h) T=285H/U_0; (i) T=300H/U_0.

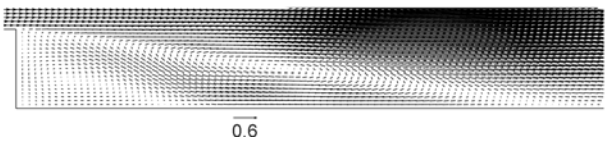

Figure 7 Time-averaged flow field behind the step.

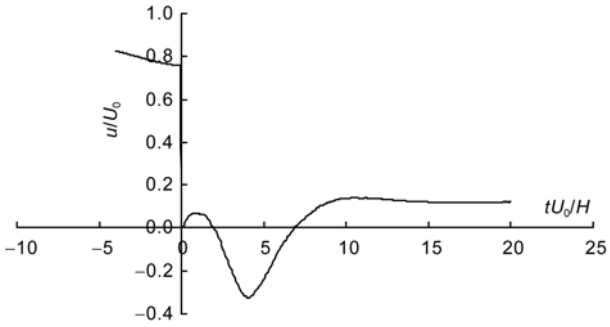

Figure 8 Horizontal velocity distribution along the step side.

lation length. Closely behind the step there still exists a small and weak eddy in the corner, whose existence is confirmed in the test. Figure 8 gives the horizontally time-averaged velocity distribution along the step side, showing that the horizontal time-averaged velocity is 0 when Xr equals 6.9H, which is the computed recirculation length. The test in ref. [15] shows Xr varies between 6H and 8H; the computational results in this paper are relatively close to the averaged test value of 7.0H.

Figure 9 gives the computational results of horizontally time-averaged velocity distribution at two cross sections behind the step, which are quite close to the test results. Figures 10 and 11 give the contour of main velocity distribution in the instantaneous and time-averaged flow fields, respectively, which can further explain the difference between the instantaneous and time-averaged characteristics of the overall flow field.

4.3 Instantaneous and time-averaged characteristics of flow field pressure

In engineering practice, the flow field pressure distribution

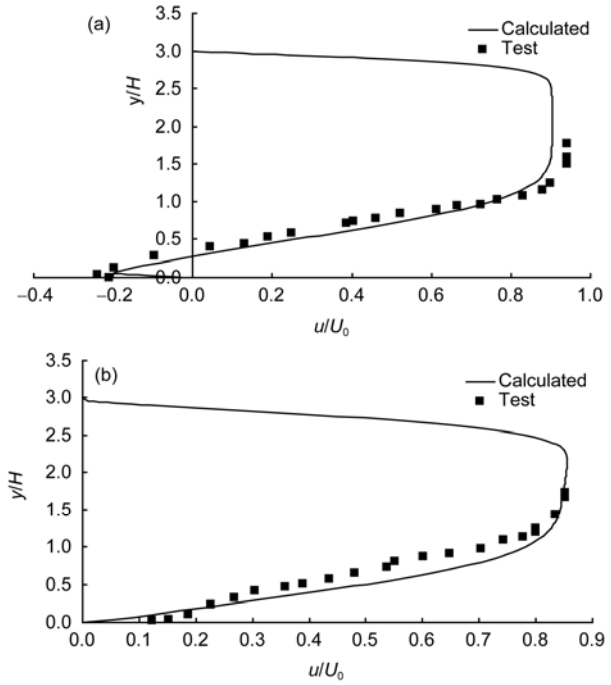

Figure 9 Horizontal time-averaged velocity distribution at the cross section behind the step. (a) x/H=5.33; (b) x/H=8.0.

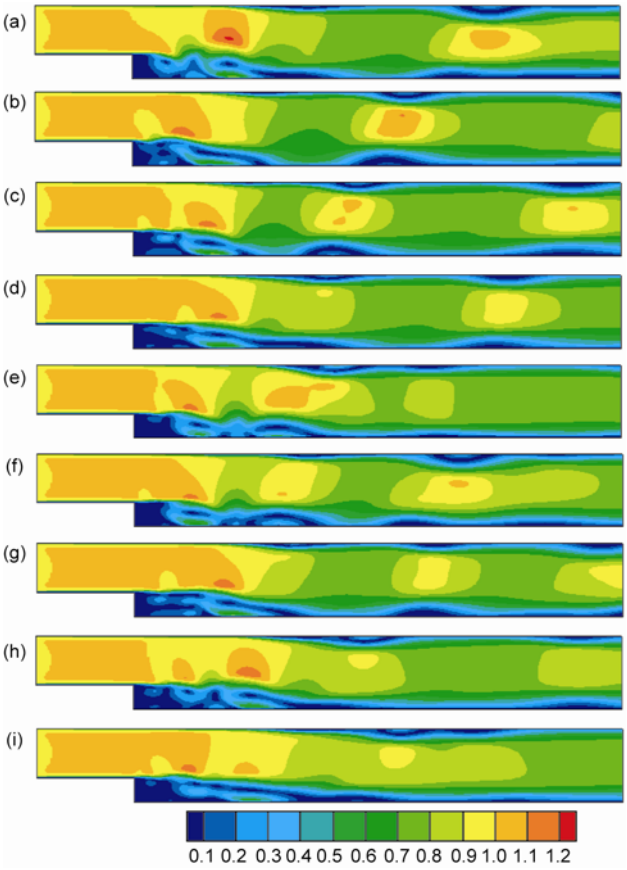

Figure 10 Contour of main velocity distribution of instantaneous flow field. (a) T=180H/U_0; (b) T=195H/U_0; (c) T=210H/U_0; (d) T=225H/U_0; (e) T=240H/U_0; (f) T=255H/U_0; (g) T=270H/U_0; (h) T=285H/U_0; (i) T=300H/U_0.

of the turbulent flow over backward-facing step at a high Reynolds number is of practical significance. Dimensionless pressure difference between probing point and reference point at the entrance, generally defined as pressure coefficient C_p, is adopted to denote pressure distribution characteristics. Computational results show that the pressure within the flow field fluctuates with time which is similar to the velocity fluctuation. Figure 12 gives the instantaneous pressure distribution when T equals 300H/U_0, indicating that the distribution is quite uneven and that in the flow field the peak and bottom values of some pressures appear at the same time. Figure 13 gives the time-averaged pressure distribution, indicating some regularity of the pressure distribution. In general, the pressure increases along the channel, inevitably leading to the separation between flow and boundary, which in turn may lead to the formation of a large eddy, around the center of which there is an obvious low-pressure area. Figure 14 gives the time-averaged pressure distribution close to the step, which is compared with the test results, showing that the two results closely behind the step are in good agreement, but the two results far away

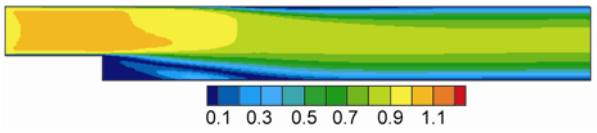

Figure 11 Contour of main velocity distribution of time-averaged flow field.

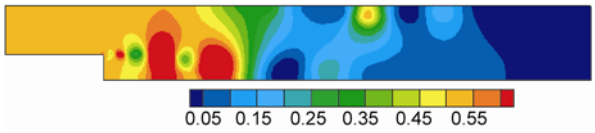

Figure 12 Instantaneous pressure field when T=300H/U_0.

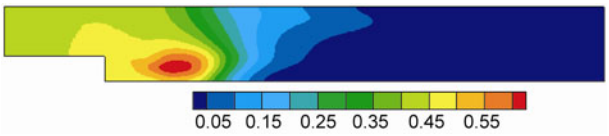

Figure 13 Time-averaged pressure field.

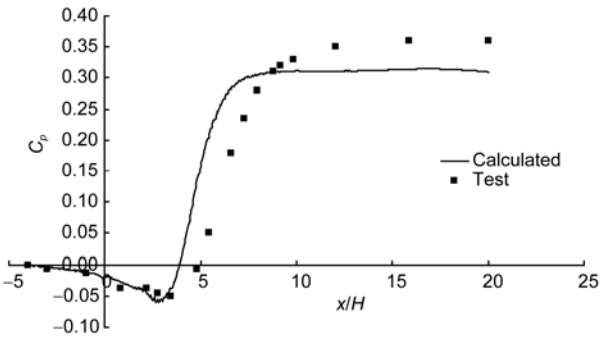

Figure 14 Pressure coefficient distribution at step side.

from the step, though the tendencies of both are similar, differ from each other to some extent.

4.4 Energy characteristics

The flow over backward-facing step belongs to the flow at sudden expansion, whose energy transport is the characteristic of sudden change. For example, the hole-plug type energy dissipater is designed based on the energy dissipation mechanism of sudden-expansion structures. Therefore, to have a better understanding of the energy transport distribution of the flow over the step is practically significant. The energy of unit volume instantaneously passing through the cross section, i.e. energy head, can be obtained in a dimensionless form by the following equation:

$$E_j = \frac{1}{q}\int_{y_d}^{y_u} U_j(P_j + U_j^2 + V_j^2)\mathrm{d}y. \tag{18}$$

By use of the above equation the time-averaged energy head $\overline{E}_j$ at all cross sections can be obtained. The time-averaged dimensionless head loss difference between check section and inflow cross section, $C_e = \overline{E}_j - \overline{E}_1$, means relative friction head loss, which can easily prove that the negative value of C_e is the head loss coefficient ξ_j in Bernoulli equation. It should be pointed out that the velocity and the pressure in the conventional computation of energy head are time-averaged values irrespective of turbulence influence. To make a comparison of the two methods, the results of the two are plotted in Figure 15, from which it can be seen that because of the effects of the large eddy behind the step, energy loss is concentrated within the region of 10*H* long behind the step, both showing a step-shaped distribution. But there is an obvious difference between the two; with the increase of the distance from the step, the turbulence intensity in flow field decreases gradually and the curves of the two become closer. All this shows that in the study of flow behind the step at a high Reynolds number, turbulence effect should not be neglected.

Currently, there are no test data to directly verify friction head loss distribution. But by the following analysis one can obtain indirect verification. It is well known to all that the local energy loss coefficient at sudden expansion derived by use of one-dimension momentum conservation theory is

$$\xi_1 = (1 - \frac{A_1}{A_2})^2 \frac{U_1^2}{2g}, \tag{19}$$

by which the local energy loss coefficient in this paper is calculated to be 0.11. From Figure 15 one can see that when x is about 10*H*, ξ_j =0.1, revealing that the computational results in this paper are believable.

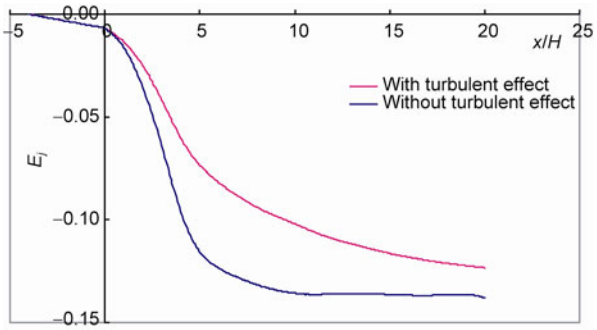

Figure 15 Relative friction head distributions.

4.5 Statistical characteristics of velocity and pressure fluctuations in flow field

The following equations can be used to define the mean square error and turbulence shear stress in fluctuation statistics:

$$\sigma_u = \sqrt{\overline{u'u'}}, \sigma_v = \sqrt{\overline{v'v'}}, \sigma_p = \sqrt{\overline{p'p'}}, \tau_{xy} = -\overline{u'v'}. \tag{20}$$

Figures 16, 17 and18 give respectively the computational results of the mean square errors of horizontal velocity fluctuation and vertical velocity fluctuation, and turbulence shear stress distribution in the flow field. It can be seen that the horizontal velocity fluctuation intensity and turbulence shear stress are comparatively large near the solid wall, similar to the distribution characteristics of pipes; the peak value of the vertical velocity fluctuation intensity is comparatively far away from the solid wall. Figure 19 gives the computational results of the max. turbulence shear stress distribution at cross section, showing that near x=3*H*, there

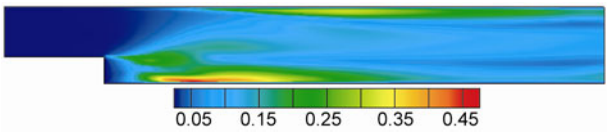

Figure 16 Computational results of mean square deviations of horizontal velocity fluctuation σ_u.

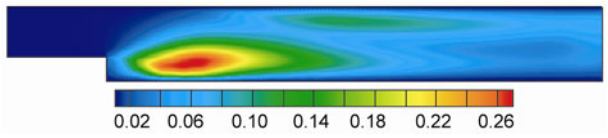

Figure 17 Computational results of mean square errors of vertical velocity fluctuation σ_v.

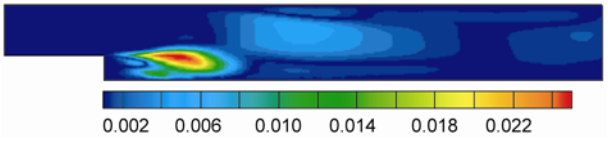

Figure 18 Turbulence shear stress distribution τ_{xy}.

is obviously a peak value of 0.015 and after x=6H, the value rapidly decreases. Compared with the test results in the figure, although the distribution tendency is similar, there is still a big difference. In the test, the peak value of 0.10 occurred near x = 7H. The cause of such difference should be further identified.

Figure 20 gives the computational results of the distribution of mean square deviation of pressure fluctuation in the flow field, showing that near the eddy center behind the step, the intensity of the pressure fluctuation is the largest. Figure 21 gives the computational results of the distribution of mean square deviation of pressure fluctuation along the step side, showing that the turbulence intensity near x=4.5H is the largest, reaching 0.24. Pressure fluctuation-induced dynamic loading plays an important role in engineering safety, and is directly related to the cavitation problems for structures under the action of high-velocity flow. The computational results of pressure fluctuation statistics in this paper should be further verified.

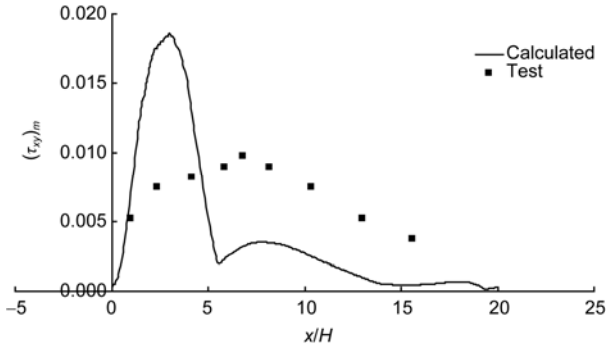

Figure 19 Computational results of the max. turbulence shear distribution at cross section.

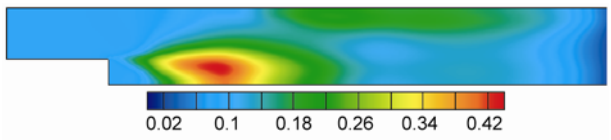

Figure 20 Computational results of the distribution of mean square error of pressure fluctuation in flow field.

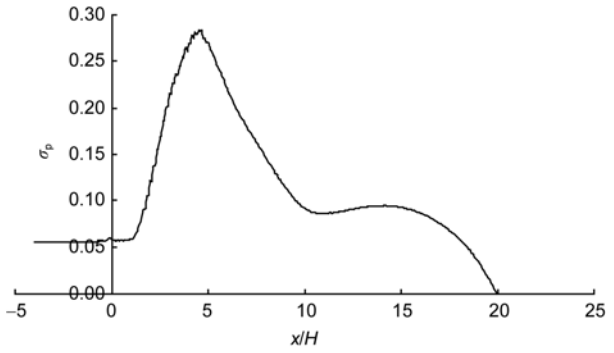

Figure 21 Computational results of mean square error of pressure fluctuation along step side.

4.6 Comparison of various computational methods

It is generally accepted that the reattachment length is an important factor for verifying the computational method. To further prove the validity of the SEL-DNS method proposed in this paper, a comparison is made of various numerical methods for the same computational case, as shown in Table 1. No. 1 shows the test data in ref. [15]; No. 2 gives the test data of the SEL-DNS method proposed by the authors; No. 3 shows the test data in ref. [13] using SEL-RAN(k-ε) method; No. 4 gives the test data in ref. [14] using FVM-RAN(k-ε) method, and No. 5 is the direct numerical solution of ref. [12] using pure Lagrange SPH method. It can be seen that the computational result of reattachment length using both SEL-DNS method and SEL-RANS(k-ε) method is close to the mean value of 7.0, that of FEM-RANS(k-ε) method is comparatively small, and that of SPH-DNS method is obviously too large. The set of computations using SEL-DNS method by PC took about 2h. As compared with RANS method, although the computational volume of SEL-DNS method increases a bit, it turns out to be in the same order of magnitude; if using SPH-DNS method, it would take 30 days by means of a super computer.

Figure 22 gives time-averaged horizontal velocity distributions at two cross sections of the eddy area behind the step, showing that the results of both SEL-DNS method and SEL-RANS method are in good agreement with those of the test, and that the operator-slitting finite element method (SEL), which is an Euler-Lagrange approach, is an efficient computational method.

Finally, it should be pointed out that as the simulation of large eddies can produce instantaneous flow field, although SEL method requires the density of the mesh to be larger than that of RANS method, it is less than that of DNS method, hence SEL method is currently regarded as a potentially promising method. It is a pity that the authors of this paper have not found the available results of the similar large eddy simulation for comparison. However, in this paper, the mesh dimension in the same order of magnitude as the RANS method was used to realize the simulation of turbulent flow by DNS method. If the coarse-grid mesh in this paper was used in LES method, the results would be interesting and meaningful. Further results obtained by the authors will be published separately.

Table 1 Comparison of reattachment lengths of various computational methods

No.	Model	Xr/H	Nodes	Computational time
1	Experiment	6–8		
2	SEL-DNS	6.9	16669	PC-2.5Hours
3	SEL-k-ε	6.8	4255	
4	FVM-k-ε	5.3	3760	
5	SPH-DNS	16.6	360482	Super Computer-30 D

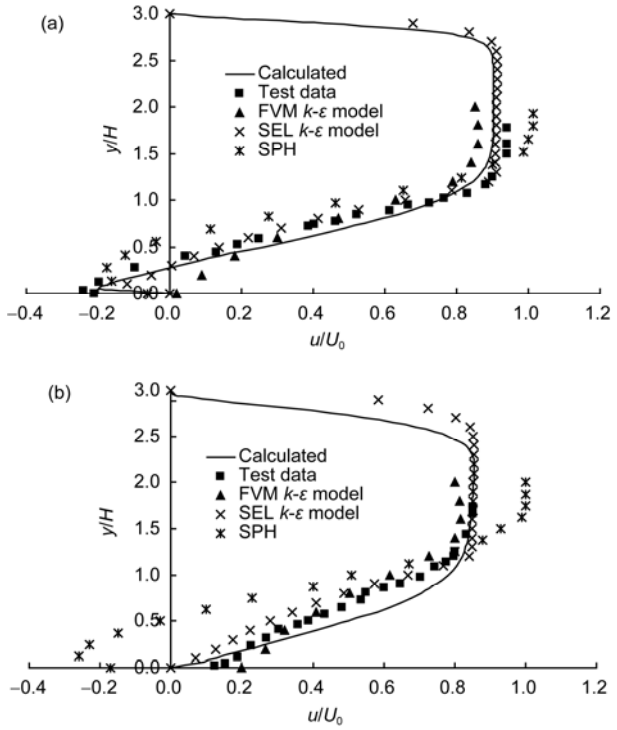

Figure 22 Time-averaged horizontal velocity distributions at two cross sections of the eddy area behind the step by various methods. (a) x/H=5.33; (b) x/H=8.0.

5 Conclusions

In this paper, direct numerical solution of N-S equation is made to simulate the flow over backward-facing step at a high Reynolds number on coarse grids, from which time-averaged flow field as well as the instantaneous and statistical characteristics of the flow field has been obtained. This makes it possible that DNS method will become a practical method to predict the complex turbulent flow controlled by large eddies in actual engineering.

The SEL-DNS method proposed by the authors of this paper uses different suitable approaches to fit different operators in N-S method, and adopts characteristic linear method to solve convection operator to avoid the difficulty in dealing with the nonlinearity of the equation, and employs finite element method to solve diffusion operator to adapt to the complex-shaped boundary. The computation shows that the computational results are in good agreement with the test data. This Euler-Lagrange numerical approach is expected to be an effective method to solve N-S equation for flow at a high Reynolds number.

The numerical test shows that the stability of the numerical simulation of flow at a high Reynolds number is far from satisfaction, and is quite sensitive to the numerical methodology and the detailed arrangement of elements. To further improve the accuracy of the numerical computation and perfect the solutions is the goal for further studies. Furthermore, turbulent flow is a three-dimensional flow, hence further in-depth researches on three-dimensional flow at a high Reynolds number controlled by large eddies need to be carried out.

This work was supported by the Major National Science and Technology Projects of China (Grant No. 2012ZX07506003) and the Public Research and Development Project for Water Resource (Grant No. 201001030).

1 Orszag S A, Patterson G S. Numerical simulation of three-dimensional homogeneous isotropic turbulence. Phys Rev Lett, 1972, 28: 76–79
2 Rogallo R S. Numerical experiments inhomogeneous turbulence. NASA TM-81315, 1981
3 Rogallo R S, Moin P. Numerical simulation of turbulent flows. Annu Rev Fluid Mech, 1984, 16: 99–137
4 Moser R D, Moin P. The effects of curvature in wall-bounded turbulent flows. J Fluid Mech, 1987, 175: 479–510
5 Spalart P R. Numerical study of sink-flow boundary layers. J Fluid Mech, 1986, 172: 307–28
6 Spalart P R. Direct numerical simulation of a turbulent boundary layer up to R_θ=1410. J Fluid Mech, 1988, 187: 61–98
7 Hung L, Parviz M, John K. Direct numerical simulation of turbulent flow over a backward-facing step. J Fluid Mech, 1997, 330: 349–374
8 Sengupta K, Mashayek F, Jacobs B. Direct numerical simulation of turbulent flows using spectral methods. 46th AIAA Aerospace Sciences Meeting and Exhibit, 7 - 10 January 2008, Reno, Nevada
9 Moin P, Mahesh K. A tool in turbulence research. Annu Rev Fluid Mech, 1998, 30: 539–78
10 Wengle H, Huppertz A, Bärwolffc G, et al. The manipulated transitional backward-facing step flow: An experimental and direct numerical simulation investigation. Eur J Mech B-Fluids, 2001, 20: 25–46
11 Lele S K. Compact finite-difference schemes with spectral-like resolution. J Comp Phys, 1992, 103:16–42
12 Ting T S, Prakash M, Cleary P W, et al. Simulation of high Reynolds number flow over a backward facing step using SPH. ANZIAM, 2006, 47(FNA): 292–309
13 Ding D Y, Wu S Q. Numerical application of κ-ε turbulence model to flow over a backward-facing step. Sci China Tech Sci, 2010, 53(10): 2817–2825
14 Zijlema M, Segal A, Wesseling P. Finite Volume Computation of 2D Incompressible Turbulent Flows in General Coordinates on Staggered Grids. Report 1994-24, Delft University of Technology
15 Kim J, Kline S J, Johnston J P. Investigation of a reattaching turbulent shear layer: Flow a backward-facing step. ASME J Fluids Eng, 1980, 102: 302–308
16 Ding D Y, Zhen P X. Numerical Simulation of Cooling Water for Yangzhou Power Plant. Technical Report, Nanjing Hydraulic Research Institute, Report No. H8837. 1988
17 Ding D Y, Wu S Q. Study on three-dimensional numerical model for shallow water flow (in Chinese). Eng Sci, 2010, 2(2): 33–40